

# Tantalum carbide as a novel support material for anode electrocatalysts in polymer electrolyte membrane water electrolysers

**Polonský, Jakub; Petrushina, Irina; Christensen, Erik; Bouzek, K.; Prag, Carsten Brorson; Andersen, Jens Enevold Thaulov; Bjerrum, Niels**

*Published in:*
International Journal of Hydrogen Energy

*Link to article, DOI:*
10.1016/j.ijhydene.2011.11.035

*Publication date:*
2012

*Document Version*
Publisher's PDF, also known as Version of record

Available online at www.sciencedirect.com

SciVerse ScienceDirect

journal homepage: www.elsevier.com/locate/he

# Tantalum carbide as a novel support material for anode electrocatalysts in polymer electrolyte membrane water electrolysers

J. Polonský [a,*], I.M. Petrushina [a], E. Christensen [a], K. Bouzek [b], C.B. Prag [a], J.E.T. Andersen [c], N.J. Bjerrum [a]

[a] Energy and Materials Science Group, Department of Chemistry, Technical University of Denmark, Kemitorvet 207, DK-2800 Kgs. Lyngby, Denmark

[b] Department of Inorganic Technology, Faculty of Chemical Technology, Institute of Chemical Technology, Prague, Technická 5, 166 28 Praha 6-Dejvice, Czech Republic

[c] Analytical Chemistry, Department of Chemistry, Technical University of Denmark, Kemitorvet 207, DK-2800 Kgs. Lyngby, Denmark

ARTICLE INFO

*Article history:*
Received 27 July 2011
Received in revised form
6 October 2011
Accepted 5 November 2011
Available online 5 December 2011

*Keywords:*
PEM water electrolysis
Electrocatalyst support
Oxygen evolution reaction
Corrosion resistance
Iridium oxide anode electrocatalyst
Tantalum carbide

ABSTRACT

Iridium oxide ($IrO_2$) currently represents a state of the art electrocatalyst for anodic oxygen evolution. Since iridium is both expensive and scarce, the future practical application of this process makes it essential to reduce $IrO_2$ loading on the anodes of PEM water electrolysers. In the present study an approach to utilising a suitable electrocatalyst support was followed. Of the materials selected from a literature review, TaC has proved to be stable under the conditions of the accelerated stability test proposed in this study. The test involved dispersing each potential support material in a mixture of trifluoromethanesulfonic acid (TFMSA) and hydrogen peroxide at 130 °C. The liquid phase was subsequently analysed using ICP-MS with respect to the occurrence of ions potentially originating from the support material tested. The TaC support selected was additionally characterised by thermogravimmetric and differential thermal analysis to prove its thermal stability. A modified version of the Adams fusion method was used to deposit $IrO_2$ on the support surface. A series of electrocatalysts was prepared with a composition of $(IrO_2)_x(TaC)_{1-x}$, where $x$ represents the mass fraction of $IrO_2$ and was equal to 0.1, 0.3, 0.5, 0.7, 0.9 and 1. The thin-film method was used for electrochemical characterisation of the electrocatalysts prepared. SEM–EDX analysis, X-ray diffraction, $N_2$ adsorption (BET) and powder conductivity measurements were used as complementary techniques to complete characterisation of the electrocatalysts prepared. The electrocatalysts with $x \geq 0.5$ showed stable specific activity. This result is consistent with the conductivity measurements.


## 1. Introduction

Hydrogen is currently considered to be one of the most important future energy carriers that can be used to store energy from renewable sources. Energy stored in hydrogen can be converted back into electricity for use in the distribution grid or in technologies such as uninterrupted power sources and hydrogen-powered cars [1,2].

* *Corresponding author*. Present address: Department of Inorganic Technology, Faculty of Chemical Technology, Institute of Chemical Technology, Prague, Technická 5, 166 28 Praha 6-Dejvice, Czech Republic. Tel.: +420 604 192 095 (mobile), fax: +420 220 444 410.
E-mail address: jpolonsky@gmail.com (J. Polonský).
0360-3199/$ – see front matter 
doi:10.1016/j.ijhydene.2011.11.035

Electrolysis is a viable method for the production of carbon-free hydrogen. Although alkaline electrolysis is currently mainly used for this purpose, acidic polymer electrolyte membrane water electrolysers (PEMWEs) are attracting great interest as a promising new alternative technology [3]. The advantages of PEMWEs over alkaline electrolysers primarily lie in their higher efficiency and higher process intensity [4]. However, the major drawback of the PEMWEs is the need for electrocatalysts based on platinum group metals. This especially concerns the anode, where so far only iridium-based electrocatalysts are known to withstand the severe conditions that occur at the PEMWE anode during the oxygen evolution reaction (OER) [5]. The highly acidic environment at the PEMWE anode, together with a polarisation of $\geq$1.5 V and temperatures of 80–200 °C, can be tolerated by few materials for any length of time [6]. Whereas $RuO_2$ has the lowest overpotential for OER, $IrO_2$ is far more stable and is, therefore, used exclusively as an oxygen evolution electrocatalyst [7].

Unfortunately, iridium is not only expensive (1085 USD/troy ounce as of 1 December 2011 [8]), but also scarce, being about 50 times less abundant than platinum [9]. In 2010, the electrochemical industry accounted for approximately one quarter of its total demand [10]. Consequently, it is crucial to reduce the amount of $IrO_2$ in PEMWEs if this technology is to become more widely used. One approach to lowering the amount of $IrO_2$ in PEMWEs involves the use of an electrocatalyst support; namely, a non-reactive material that is preferably both inexpensive and readily available [11]. The role of the electrocatalyst support in this process can be threefold. Firstly, it enables synthesis of smaller $IrO_2$ crystallites because it offers a number of crystallisation centres during $IrO_2$ deposition and at the same time reduces the probability of their agglomeration. Secondly, supported particles are larger in size than unsupported particles. This is advantageous during preparation of the catalytic layer: larger particles do not penetrate deeper into the layer, but stay in good contact with the polymer electrolyte membrane. As a consequence, higher efficiency of electrocatalyst utilisation can be achieved. Thirdly, the interaction of the electrocatalyst with the support may influence the electrocatalytic properties of the resulting material due to synergic effects.

Building on the work of Nikiforov et al., who have shown that SiC–Si can be used as an electrocatalyst support [12], this work focused on ceramic materials. Four ceramic materials potentially suitable for this application were identified in the literature [13]: TaC, $Si_3N_4$, WB and $Mo_2B_5$. These materials were chosen because they are stable in harsh environments and also, in some cases, are electrically conductive. To select the most stable material in this group, a quick and easy preliminary stability test was developed, based on exposing the prospective support material to a mixture of trifluoromethanesulfonic acid (TFMSA) and hydrogen peroxide at 130 °C. After a defined time, the liquid phase is analysed for the presence of ions originating from the dissolved support material. TFMSA was chosen because it provides a high level of acidity without any unwanted complexing or chelating effects. The hydrogen peroxide provides an oxidative environment to simulate the anodic polarisation in a PEMWE. Overall, the conditions chosen were harsher than conditions in a PEMWE because this is an accelerated test which should provide the required information on material stability in a relatively short time.

Electronic conductivity represents another important parameter that influences electrocatalyst performance. At this point a distinction has to be made between the conductivity of the support itself and of the entire composite material, consisting of the support and $IrO_2$. It should be borne in mind that the conductivity of $IrO_2$ alone is sufficient for the operation of a PEMWE when $IrO_2$ covers most of the support, *i.e.* when it exceeds the percolation level. Therefore, even a non-conductive support may be acceptable for the process. However, it is necessary to use high $IrO_2$ loading and at the same time a support material with a relatively low specific surface area to allow formation of a coherent conductive surface film of $IrO_2$. Finally, the electrical conductivity of the support is very welcome since it can reduce the ohmic drop in the PEMWE [14], but it is not a critical quality.

Several methods for the synthesis of electrocatalysts have been described in the literature. The most common is the Adams fusion method [15], which produces metal oxides [12,16–20]. The other methods used are the polyol method (also known as the colloid method) [16,17,19], simple thermal decomposition of the corresponding metal chlorides [21], and chemical reduction [22]. The polyol method and chemical reduction are usually followed by the oxidation of the resulting metal particles, either anodically or by simple calcination in air.

In the present work a modified version of the Adams fusion method was used for the synthesis of $IrO_2$ supported on TaC. This method was selected because it provides $IrO_2$ particles straight from the synthesis and because it allows direct comparison with the results of the preceding work [12]. The electrochemical activity of the prepared supported $IrO_2$ electrocatalysts was compared with that of an unsupported $IrO_2$ electrocatalyst.

Thus, for the first time, the use of TaC as a support material for $IrO_2$-based electrocatalysts for PEMWEs is reported.

## 2. Experimental

### 2.1. *Support stability testing*

#### 2.1.1. *Starting materials*

Based on a literary review, the following materials were tested as potential electrocatalyst supports: TaC (Sigma–Aldrich, 99%), $Si_3N_4$ (Goodfellow, >85%), WB (Alfa Aesar, 99%) and $Mo_2B_5$ (Cerac Inc., 99.5%). To remove any surface contamination, approximately 200 mg of each material was first etched in 50 mL of boiling 2% HCl for 15 min. After cooling down to room temperature, each suspension was washed five times with demineralised water on a centrifuge to remove chlorides. Final washing was followed by evaporation under argon.

#### 2.1.2. *Chemical stability test of the support*

A mixture of the four support materials was created by taking 50 mg of each one. Then, 5 mL of concentrated TFMSA (Sigma–Aldrich, 98%) was poured into the mixture before 1.67 mL of 30% hydrogen peroxide was added drop-wise. The mixture was kept stirred at 130 °C in a glass vessel, at the top of which

a reflux condenser was attached. After 48 h, the mixture was cooled down to room temperature and diluted to 50 mL with demineralised water. The remaining powder was separated using a centrifuge and a 5 mL aliquot was taken as a sample. To prevent the ions from precipitating, 100 mg of NaF was added to the sample and the mixture was heated in a closed vessel at 80 °C for 1 h.

#### 2.1.3. *ICP-MS analysis*

The sample containing the dissolved ions was analysed using a Perkin–Elmer Elan 6000 ICP-MS with a dual-stage detector with a high-concentration setting. All standards for the calibration line were purchased from Fluka. The calibration line was designed with a lower limit corresponding to 0.1% of the dissolved support material.

### 2.2. *Electrocatalysts preparation*

From the stability test, TaC was chosen as the preferred electrocatalyst support. The electrocatalysts with varying content of $IrO_2$ were prepared, using a modified version of the Adams fusion method [15]. The chemical reactions (1, 2), corresponding to the Adams fusion suggested by Marshall et al. [16], are shown below:

$$H_2IrCl_6 + 6NaNO_3 \rightarrow 6NaCl + Ir(NO_3)_4 + 2HNO_3 \quad (1)$$

$$Ir(NO_3)_4 \rightarrow IrO_2 + 4NO_2 + O_2 \quad (2)$$

The TaC support and a metal precursor ($H_2IrCl_6.4H_2O$, Alfa Aesar, 99%) were added to 10 mL of isopropanol and stirred for 1 h to ensure complete dissolution of the iridium salt. After the addition of finely ground $NaNO_3$ (16.7 × molar excess), the salt mixture was heated in air to 70 °C and evaporated to dryness. Then, the mixture was placed into a furnace and heated up to 500 °C at a rate of 250 °C/h. It remained at 500 °C for 1 h before cooling to room temperature overnight. The fused product was washed six times with demineralised water and separated on a centrifuge. Finally, the powder was dried in air at 90 °C.

Electrocatalysts were prepared with concentrations of 10, 30, 50, 70, 90 and 100 wt.% $IrO_2$ and are labelled as $(IrO_2)_x(TaC)_{1-x}$, where $x$ is the mass fraction of $IrO_2$. Like all Adams fusion processes, our modified version provided a yield of almost 100% [16]. The modified Adams fusion process was also applied to pure TaC to see if the process had any impact on its properties.

### 2.3. *Physico-chemical characterisation*

Scanning electron microscope (SEM) images of the electrocatalysts were taken on a JEOL JSM-5910 (10 kV acceleration voltage, 7 mm working distance). The SEM was equipped with an energy-dispersive X-ray spectrometer (EDX) that was used to collect an element map of the electrocatalyst. The EDX itself consisted of an Oxford Instruments X-Max silicon drift detector (SDD) controlled by Oxford Instruments INCA software.

A Netzsch STA 409 PC was used to perform thermogravimmetric and differential thermal analysis on the TaC. In a synthetic air atmosphere (20.8% $O_2$, 79.2% $N_2$, AGA GAS AB), the temperature ramp was increased from room temperature to 1000 °C at a rate of 5 °C/min.

All electrocatalyst samples were analysed on a Huber D670 X-ray powder diffractometer (Cu–K$\alpha$, $\alpha = 1.5405981$ Å).

Using a Micromeritics Gemini 2375 analyser, the specific surface areas of the electrocatalysts and the TaC were measured by the Brunauer–Emmett–Teller (BET) method.

In accordance with a method previously used by our group [12], powder conductivity measurements were performed in a small acrylic cylinder with a through hole (inner diameter 3 mm) into which two opposing copper pistons retracted. The powder was compressed in the cell by clamping the outer ends of both pistons in a micrometre. The micrometre axle was tightened to a constant torque of 0.2 Nm. Then, a VersaSTAT 4 potentiostat running VersaStudio 2.0 software (Princeton Applied Research) was used to determine the conductivity of the powder samples. Conductivity of each sample was measured for 4–5 layer thicknesses. The conductivity value was obtained from the slope of the dependence of its resistance on thickness.

### 2.4. *Electrochemical characterisation*

To evaluate the electrochemical performance of the electrocatalysts, working electrodes were prepared using the thin-film method [23]. A glassy-carbon disk embedded in PTFE casing was used as the working electrode. The exposed part consisted of a 5 mm diameter circle onto which was pipetted 8 μL of electrocatalyst dispersion in demineralised water, the dispersion having been ultrasonically homogenised for 1 h beforehand. For all samples, the $IrO_2$ concentration in the dispersion was 1 mg per mL. The electrocatalyst loading on the working electrode was 40 μg of $IrO_2/cm^2$. The electrocatalyst layer was fixed with an 8 μL drop of diluted Nafion solution (1 mg dry basis/mL) in isopropanol/demineralised water (3:1, w/w).

Electrochemical measurements were carried out in a three-necked electrochemical cell with a platinum wire counter-electrode and a saturated calomel reference electrode (SCE) connected to the cell via a liquid junction. All potentials in this article refer to this electrode. The electrolyte was 0.5 M $H_2SO_4$ at room temperature (23 ± 2 °C).

A VersaSTAT 4 potentiostat running VersaStudio 2.0 software (Princeton Applied Research) was used for all electrochemical experiments. Cyclic voltammetry experiments were conducted between 0 and 1.2 V at scan rates of 500, 300, 100 and 50 mV/s. Tafel experiments were performed from 1.1 to 1.3 V at a scan rate of 1 mV/s.

## 3. Results and discussion

### 3.1. *Support stability test*

The solution analysis detected the most unstable compound of the four analysed to be $Mo_2B_5$, which had the highest dissolution extent of 93.3%. On the other hand only 3.3% of WB dissolved in 48 h. This material thus proved to be relatively stable under test conditions. But although such a relatively

slow dissolution was detected, it may represent a problem in PEMWE, where the material must be able to withstand thousands of runtime hours. According to the analysis, only 0.5% of $Si_3N_4$ dissolved within 48 h of exposure. This suggests that it is highly stable. Additionally, the effect of the nitrogen present in the air and Si from the glass reaction vessel walls on the analysis results has to be considered. This material thus represents a promising candidate for the electrocatalyst support. But the results of the ICP-MS analysis showed that TaC, with no ions detected in the solution (Table 1), was the most resistant material of those under study. Therefore TaC was chosen as the support for $IrO_2$ in this study.

To confirm the thermal stability of TaC selected as the electrocatalyst support, TGA and DTA curves were recorded for the as-received sample of this material (Fig. 1). TaC showed a steady weight gain above 200 °C as it was oxidised to $Ta_2O_5$. At 330 °C, oxidation to $Ta_2O_5$ had reached an extent of 1 wt.%. More rapid oxidation started at temperatures above 600 °C and finished at 790 °C. At this point TaC was quantitatively oxidised to $Ta_2O_5$. Theoretically, 100% TaC oxidised to $Ta_2O_5$ should show a weight gain of 14.5 wt.%. A gain of 14.9 wt.%, calculated as the difference between the lowest and highest recorded mass, was observed within this study. This discrepancy may have been caused by the non-stoichiometric composition of the TaC used [24]. Thus, TaC appears to be highly stable within the temperature range foreseen for the PEMWE, *i.e.* below 200 °C. The situation is less clear with respect to electrocatalyst synthesis by Adams fusion. Here $Ta_2O_5$ formation has to be considered as a possible option.

### 3.2. *Physico-chemical characterisation*

#### 3.2.1. *X-ray diffraction*

X-ray diffractograms of series of the electrocatalysts based on TaC supported $IrO_2$ are shown in Fig. 2. As expected, all diffractograms show well-defined lines of $IrO_2$ and TaC (except the one for pure $IrO_2$). Besides these lines, an additional component, identified as $NaTaO_3$, was observed in the diffraction spectra of the supported electrocatalyst: it is a perovskite-type semiconductor with a band gap of 4.0 eV [25]. Its origin lies in oxidation of the TaC support by $NaNO_3$ during the Adams fusion process. Diffraction lines of this component are scarcely visible for the electrocatalyst containing 90% of $IrO_2$. This is due to its small content in this particular sample. However, closer inspection reveals a definite diffraction line at $2\theta = 22.8°$.

**Table 1 – – Extent of dissolution of tested materials in $TFMSA/H_2O_2$ (3:1, w/w). Temperature 130 °C, duration 48 h.**

| Compound | Dissolved portion (%) |
|---|---|
| TaC | Below quantification limit (<0.1) |
| $Si_3N_4$ | 0.5 |
| WB | 3.3 |
| $Mo_2B_5$ | 93.3 |

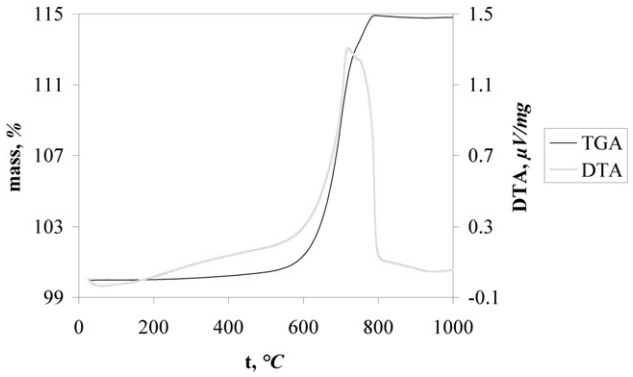


**Fig. 1 – Thermogravimmetric and differential thermal analysis curves of TaC in synthetic air. Heating rate 5 °C/min.**

The Scherrer equation [26] was used to calculate the average crystallite size of the $IrO_2$ in the electrocatalysts for different contents of $IrO_2$ (Fig. 3); the $IrO_2$ peak located at $2\theta = 28°$ (110) was used for this purpose (see inset in Fig. 2). The accuracy of this size determination was better than ±10%. The peak recorded for the 10 wt.% $IrO_2$ electrocatalyst was too weak. Therefore, the crystallite size could not be determined for this composition.

The data shown in Fig. 3 have to be discussed as two sets of data obtained under different conditions. Whereas the pure $IrO_2$ was synthesised in an initially homogeneous phase of molten salts, samples with the electrocatalyst support represent a heterogeneous reaction system where the support participates in the synthesis as a solid phase. Pure $IrO_2$ has to overcome a significant initiation barrier during nucleation of the first crystallites in the homogeneous liquid phase. Once the nucleation centres have formed, it is energetically favourable for the $IrO_2$ phase to deposit continuously on already existing crystallites. On the other hand, the presence of the electrocatalyst support introduces a high number of potential $IrO_2$ nucleation centres on the defects of its structure. Logically, pure $IrO_2$ forms larger crystallites when compared to the supported electrocatalysts.

Another interesting observation is that the smallest crystallites were observed for the 90 wt.% $IrO_2$ electrocatalyst. The higher the concentration of the support, the larger the crystallite size with pronounced enlargement starting at 50 wt.% $IrO_2$. The same trend has been reported elsewhere [16]. Such behaviour may be explained by the driving force for the nucleation of the $IrO_2$ phase: for the 90 wt.% $IrO_2$ electrocatalyst, the concentration of the iridium oxide precursor in the reaction system is the highest, resulting in the formation of the highest number of nucleation centres. Therefore, it leads to the formation of smaller crystallites. With decreasing content of the iridium oxide precursor, this driving force, and thus the number of nucleation centres formed, decreases.

#### 3.2.2. *SEM and EDX analysis*

SEM pictures of the TaC supported electrocatalyst containing 50 wt.% $IrO_2$ (Fig. 4) and the pure $IrO_2$ electrocatalyst (not shown) were recorded. The morphology of the two samples is similar, both showing $IrO_2$ present in the form of

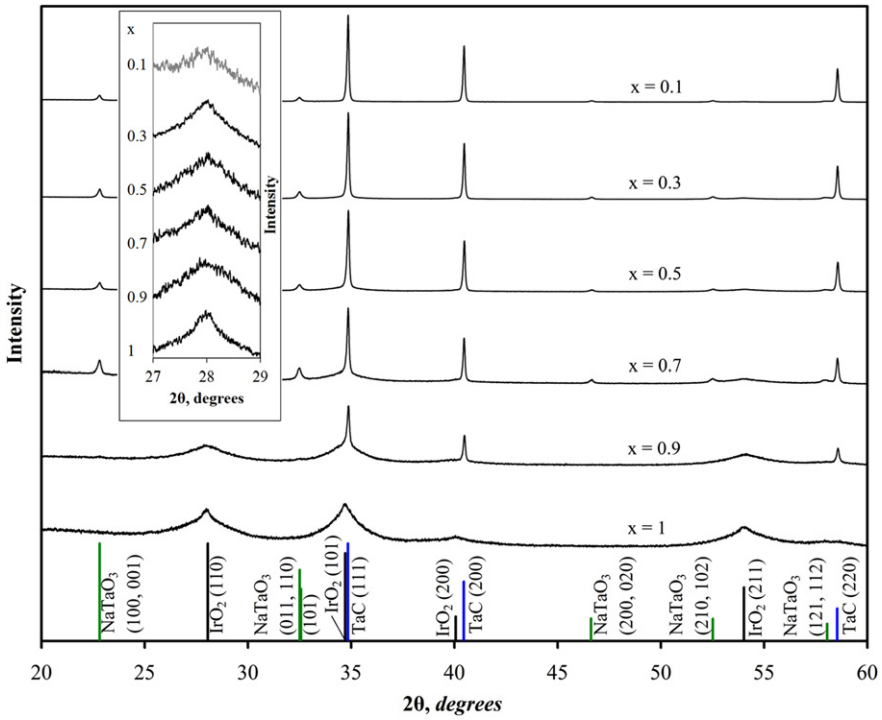


**Fig. 2 – X-ray diffractograms of electrocatalysts prepared with mass-based composition $(IrO_2)_x(TaC)_{1-x}$. Figures in parentheses indicate corresponding *h*, *k*, *l* Miller indices of the crystal planes. The inset graph shows zoomed region around 28° where the characteristic peak of $IrO_2$ has been used to calculate the crystallite size.**

agglomerates ranging from 50 to 500 nm in diameter. Owing to the rounded shape of the agglomerates, the surface-to-mass ratio is relatively high, enabling high electrocatalytic activity. The homogeneity of the $IrO_2$ distribution is confirmed by the EDX element map (Fig. 5).

The sodium content was determined to confirm the presence of the $NaTaO_3$ phase formed during Adams fusion and identified by XRD experiments. Homogeneous distribution over the support surface was proven (Fig. 5).

### 3.2.3. *Specific surface area*

Of the materials studied, pure $IrO_2$ had the highest specific surface area (SSA) of 121 $m^2/g$, while pure TaC had the lowest one at only 2.4 $m^2/g$ for TaC after synthesis (Fig. 6) and 0.7 $m^2/g$ as-received (not shown). The remaining samples followed the rule of mixing, *i.e.* the SSA was linearly dependent on the content of $IrO_2$ in the sample. No relation between crystallite size and SSA was observed. This is further confirmed by the SSA of the $IrO_2$ part in the supported electrocatalyst calculated from the known SSA of the support and composition of the sample. The results (Fig. 6) indicate no dependence on the size of the $IrO_2$ crystallites. From the SEM image (Fig. 4) and XRD analysis (Fig. 3), it can be concluded that the individual

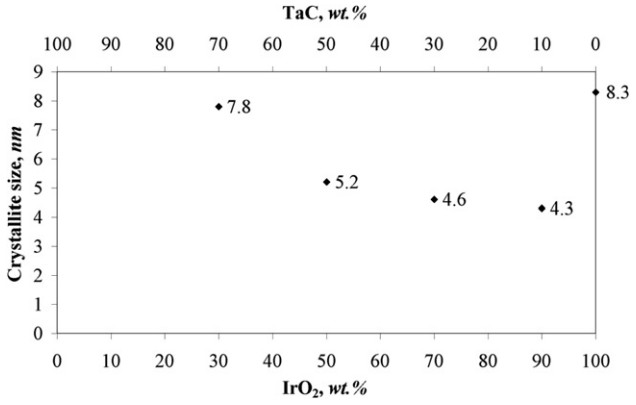


**Fig. 3 – Average crystallite sizes of the prepared electrocatalysts as calculated from the XRD spectra.**

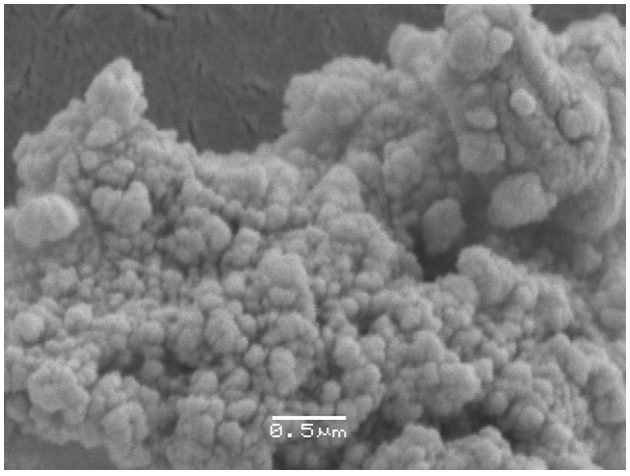


**Fig. 4 – Detailed SEM image of 50 wt.% $IrO_2$ electrocatalyst. Accelerating voltage 10 kV, working distance 7 mm.**

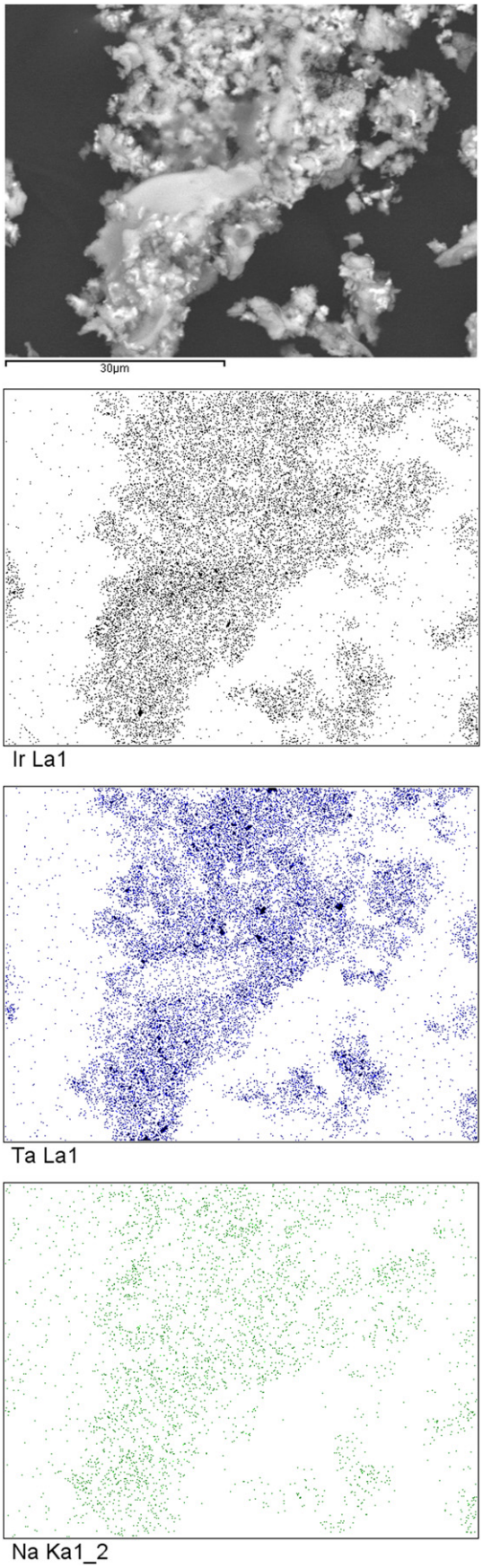


**Fig. 5 – SEM–EDX element map for 50 wt.% $IrO_2$ electrocatalyst.**

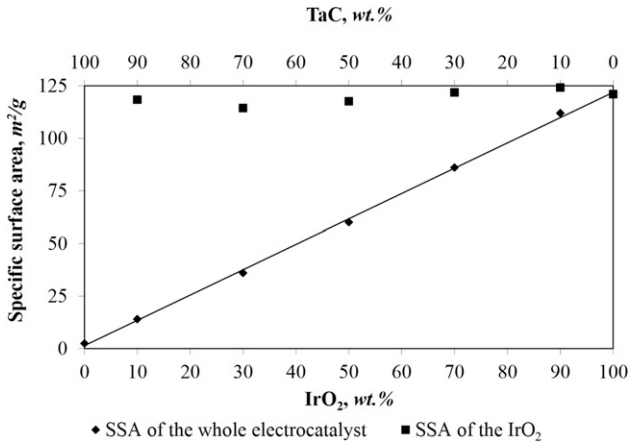


**Fig. 6 – BET specific surface area of the prepared electrocatalysts.**

crystallites are 1–2 orders of magnitude smaller than the agglomerates. Since no relation between SSA and crystallite size was found, it is concluded that the agglomerates are not porous and the adsorbent gas cannot access inner surfaces. Furthermore, with respect to the size variations observed (Fig. 3), it appears that crystallite size does not influence the shape and morphology of the agglomerates and, therefore, does not affect the SSA.

### 3.2.4. *Powder conductivity*

First of all, when comparing the presented results with published data it should be borne in mind that powder conductivity is strongly dependent on the conditions under which it is obtained. This is because the transition resistance between the individual powder particles plays a decisive role. From this, it follows that the most important aspect is particle dimensions and compressive force. Therefore, for instance, for bulk TaC a conductivity of 23–34 $\times$ $10^3$ S/cm has been reported [13]. The conductivity of the as-received TaC powder used in this study was 118 S/cm. This difference is clearly due to the fact that TaC was used in powdered form. Compared to

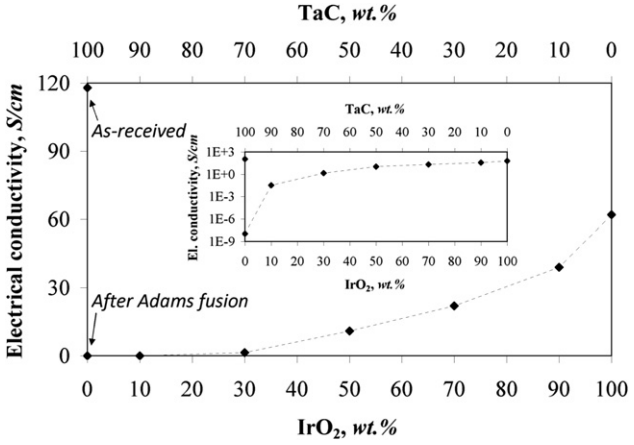


**Fig. 7 – Powder conductivities of the prepared electrocatalysts. The inset graph shows conductivities with a logarithmically scaled y-axis.**

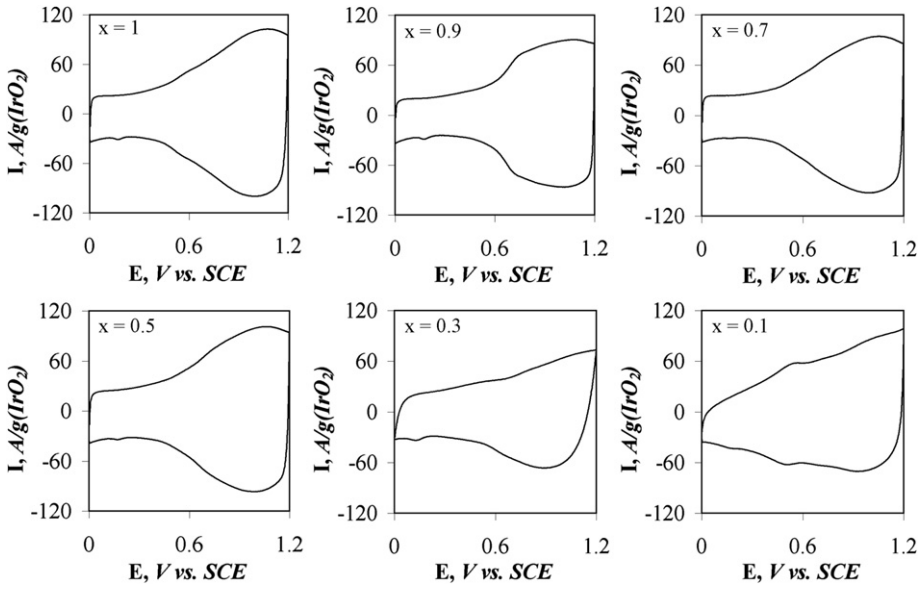


**Fig. 8 – Cyclic voltammograms normalised to $IrO_2$ mass-specific current. Mass-based compositions correspond to general formula $(IrO_2)_x(TaC)_{1-x}$. Potential sweep rate 500 mV/s, 0.5 M $H_2SO_4$ at room temperature.**

pure $IrO_2$ powder, which had a conductivity of 62 S/cm, the as-received TaC powder was twice as conductive. Unfortunately, after synthesis, the conductivity of the TaC decreased by 10 orders of magnitude. Coming back to the above reported data, the drop in conductivity can be explained by the surface layer of a semiconductive $NaTaO_3$ formed during $IrO_2$ synthesis by Adams fusion. Since surface oxidation is directly linked to the use of this synthesis method, the employment of a different method may reduce or even prevent this drop in conductivity entirely. The dependence of materials-specific conductivity on its composition is summarised in Fig. 7. As shown in the logarithmic scale presented in the figure inset, the most pronounced conductivity increase occurs with the first $IrO_2$ addition to the support. This could be due to the interaction of the $NaTaO_3$ covering the support surface with Ir atoms, most probably directly during the fusion. Even though the increase in conductivity had already reached several orders of magnitude at this stage, sufficient conductivity values of at least 10% of the conductivity of pure $IrO_2$ were first obtained with an $IrO_2$ content of 50 wt.%. This corresponds to the formation of a conductive $IrO_2$ film covering the surface of the support.

### 3.3. *Electrochemical characterisation*

#### 3.3.1. *Cyclic voltammetry*

The cyclic voltammograms of the $IrO_2$-based electrocatalysts (Fig. 8) had the overall shape that has been reported by other researchers [21,27]. This shape is characterised by an absence of any well-defined peaks, although the total anodic charge recorded is related to the total number of active sites [11]. A reliable, generally accepted electrochemical method of determining the active area, as it has for example been established for platinum, has not yet been found for iridium oxide.

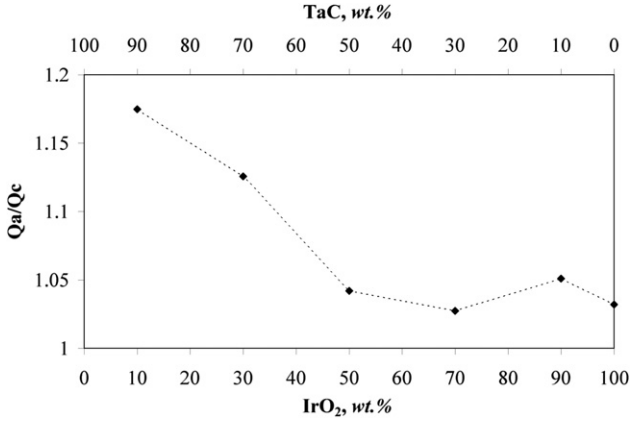


**Fig. 9 – Ratio of anodic-to-cathodic charge between 0.4 and 1.2 V. Potential sweep rate 500 mV/s, 0.5 M $H_2SO_4$ at room temperature.**

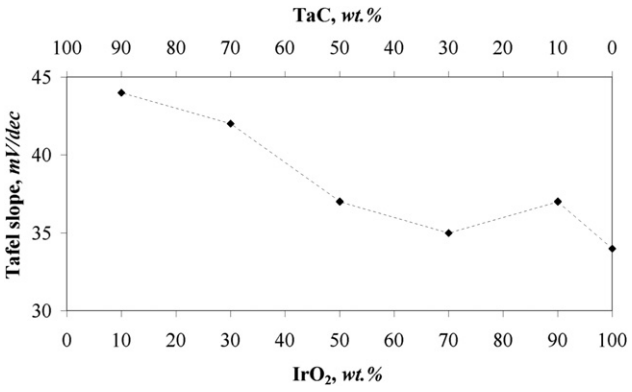


**Fig. 10 – Tafel slopes of the prepared electrocatalysts. From linear part of the polarisation curve in Tafel plot between 1.1 and 1.3 V. Potential sweep rate 1 mV/s, 0.5 M $H_2SO_4$ at room temperature.**

In the potential region between 0.4 and 1.2 V, the anodic and cathodic parts of the voltammograms display a high degree of symmetry. The predominant influence of $IrO_2$ on the voltammetric response of the electrode is indicated by the anodic-to-cathodic charge ratio (Qa/Qc) being close to unity [28]. In the present study this charge was integrated for the potential range between 0.4 and 1.2 V, where the polarisation curve is not influenced by gas evolution reactions or adsorption processes. Polarisation curves obtained at a scan rate of 500 mV/s were used to obtain higher current densities and thus a lower relative error of the experimental data. The results are summarised in Fig. 9. They are in agreement with the work of Marshall et al. [14], who observed that the higher the scan rate, the higher the differences between the charge ratios of the electrocatalysts being compared. In the present case, the ratio value was close to unity for electrocatalysts with $\geq$50 wt.% $IrO_2$. The ratio was very close to that of pure $IrO_2$. When the content of the $IrO_2$ was reduced below 50 wt.%, the ratio increased, indicating enhanced interaction of the support with the electrolyte. This result correlates well with the conductivity measurements.

#### 3.3.2. *Tafel experiments*

Pseudostationary linear sweep voltammetry was used to determine the Tafel slopes for the individual electrocatalysts (Fig. 10). Tafel slopes are an indicator of electrocatalyst quality: the lower the Tafel slope, the faster the kinetics of the reaction and the more active the electrocatalyst (under constant electrocatalyst load conditions). Electrocatalyst activity towards oxygen evolution as a desired electrode reaction was measured.

In acidic electrolyte, several possible reaction mechanisms of the oxygen evolution reaction have been proposed [29,30]. The Tafel slope cannot be used to directly identify the reaction pathway, but it may be used to determine the rate-determining step in an assumed mechanism. However, this is not straightforward as the symmetry factor in the kinetic equations is usually not known and the considered value of 0.5 is not necessarily accurate under the conditions studied [30]. Moreover, in the present case the electrocatalysts consist of agglomerates. They probably have different reaction sites. Therefore, different rate-determining steps for different reaction sites can coexist and the measured Tafel slope then represents an average. A Tafel slope of 30 mV/dec points to the second step in the "oxide path", reaction (2) [31], and a Tafel slope of 40 mV/dec suggests that the second step in the "electrochemical oxide path", reaction (4) [31], is rate-determining.

Oxide path [30]:

$$(1)\quad S + H_2O \rightarrow S{-}OH + H^+ + e^-$$

$$(2)\quad 2S{-}OH \rightarrow S{-}O + S + H_2O$$

$$(3)\quad 2S{-}O \rightarrow 2S + O_2$$

The electrochemical oxide path has identical steps (1) and (3). It differs in step (2), which in this case can be described by reaction (4) [30]:

$$(4)\quad S{-}OH \rightarrow S{-}O + H^+ + e^-$$

Again, when the $IrO_2$ content ranged from 50 to 100 wt.%, the Tafel slopes obtained were similar for all electrocatalysts under study (34–37 mV/dec). But when the $IrO_2$ concentration was 10 or 30 wt.%, the Tafel slope increased to above 40 mV/dec, indicating a different rate-determining step. This increase correlates with the conductivity and cyclic voltammetry measurements. A similar effect was also observed by Marshall et al. [14].

## 4. Conclusions

In this study it has been shown that TaC represents a promising candidate for application as an $IrO_2$ electrocatalyst support for the anodic oxygen evolution reaction in the PEMWE. The negative aspect represented by the formation of a surface film of $NaTaO_3$, characterised by low conductivity, may be overcome by applying a sufficient amount of $IrO_2$, in this particular case 50 wt.% or more. Such a supported electrocatalyst shows properties similar to those of pure $IrO_2$, including electrocatalytic activity and the rate-determining step of the oxygen evolution reaction. The inertness of the support to the environment in electrocatalysts with $IrO_2$ content of 50 wt.% or more is further confirmed in cyclic voltammetry experiments by the ratio of pseudocapacitative charge passed through the electrode being very close to the value of pure $IrO_2$. The prepared electrocatalysts have to be tested in a PEMWE to confirm their properties under conditions of a real water electrolysis process.

## Acknowledgements

Financial support is acknowledged from the European Commission within the 7th Framework Programme (Project 212903, WELTEMP), the Danish Council for Strategic Research (Center for Renewable Hydrogen Cycling, HyCycle, Contract No. 2104-07-0041) and the Erasmus EU Student Mobility Programme.

## REFERENCES

[1] National Hydrogen Energy Roadmap [Internet]. Based on the results of the National Hydrogen Energy Roadmap Workshop. Washington, DC: U.S. Department of Energy [cited 2011 Sep 13]. Available from: http://www1.eere.energy.gov/hydrogenandfuelcells/pdfs/national_h2_roadmap.pdf; 2002.

[2] Mathias MF, Makharia R, Gasteiger HA, Conley JJ, Fuller TJ, Gittleman CJ, et al. Two fuel cell cars in every garage? Electrochem Soc Interface 2005;14:24–35.

[3] Grigoriev SA, Porembsky VI, Fateev VN. Pure hydrogen production by PEM electrolysis for hydrogen energy. Int J Hydrogen Energy 2006;31:171–5.

[4] Lu PWT, Srinivasan S. Advances in water electrolysis technology with emphasis on use of the solid polymer electrolyte. J Appl Electrochem 1979;9:269–83.

[5] Hu JM, Zhang JQ, Cao CN. Oxygen evolution reaction on $IrO_2$-based DSA® type electrodes: kinetics analysis of Tafel lines and EIS. Int J Hydrogen Energy 2004;29:791–7.
[6] Nikiforov AV, Petrushina IM, Christensen E, Tomás-García AL, Bjerrum NJ. Corrosion behaviour of construction materials for high temperature steam electrolysers. Int J Hydrogen Energy 2011;36:111–9.
[7] Valdez TI, Billings KJ, Sakamoto J, Mansfeld F, Narayanan SR. Iridium and lead doped ruthenium oxide catalysts for oxygen evolution. ECS Trans 2009;25:1371–82.
[8] Platinum Today: Price Charts [Internet]. London: Johnson Matthey Plc. [cited 2011 Dec 1]. Available from: http://www.platinum.matthey.com/pgm-prices/price-charts; 2011.
[9] Renner H, Schlamp G, Kleinwächter I, Drost E, Lüschow HM, Tews P, et al. Platinum group metals and compounds. In: Elvers B, editor. Ullmann's encyclopedia of industrial chemistry. Weinheim: Wiley-VCH Verlag GmbH & Co. KGaA; 2005. p. 13.
[10] Butler J. Platinum 2011 [Internet]. Royston: Johnson Matthey Plc [cited 2011 Sep 13]. Available from: http://platinum.matthey.com/uploaded_files/PT_2011/complete_publication.pdf; 2011.
[11] Comninellis C, Vercesi GP. Characterization of DSA oxygen evolving electrodes: choice of a coating. J Appl Electrochem 1991;21:335–45.
[12] Nikiforov AV, Tomás-García AL, Petrushina IM, Christensen E, Bjerrum NJ. Preparation and study of $IrO_2$/SiC–Si supported anode catalyst for high temperature PEM steam electrolysers. Int J Hydrogen Energy 2011;36:5797–805.
[13] Martienssen W, Warlimont H, editors. Springer handbook of condensed matter and materials data. Berlin: Springer; 2005.
[14] Marshall A, Børresen B, Hagen G, Tsypkin M, Tunold R. Electrochemical characterisation of $Ir_xSn_{1-x}O_2$ powders as oxygen evolution electrocatalysts. Electrochim Acta 2006;51:3161–7.
[15] Adams R, Shriner RL. Platinum oxide as a catalyst in the reduction of organic compounds. III. Preparation and properties of the oxide of platinum obtained by the fusion of chloroplatinic acid with sodium nitrate. J Am Chem Soc 1923;45:2171–9.
[16] Marshall A, Børresen B, Hagen G, Tsypkin M, Tunold R. Preparation and characterisation of nanocrystalline $Ir_xSn_{1-x}O_2$ electrocatalytic powders. Mater Chem Phys 2005;94:226–32.
[17] Song S, Zhang H, Ma X, Shao Z, Baker RT, Yi B. Electrochemical investigation of electrocatalysts for the oxygen evolution reaction in PEM water electrolyzers. Int J Hydrogen Energy 2008;33:4955–61.
[18] Cheng J, Zhang H, Ma H, Zhong H, Zou Y. Preparation of $Ir_{0.4}Ru_{0.6}Mo_xO_y$ for oxygen evolution by modified Adams' fusion method. Int J Hydrogen Energy 2009;34:6609–13.
[19] Cheng J, Zhang H, Ma H, Zhong H, Zou Y. Study of carbon-supported $IrO_2$ and $RuO_2$ for use in the hydrogen evolution reaction in a solid polymer electrolyte electrolyzer. Electrochim Acta 2010;55:1855–61.
[20] Wu X, Tayal J, Basu S, Scott K. Nano-crystalline $Ru_xSn_{1-x}O_2$ powder catalysts for oxygen evolution reaction in proton exchange membrane water electrolysers. Int J Hydrogen Energy 2011;36:14796–804.
[21] Marshall AT, Haverkamp RG. Electrocatalytic activity of $IrO_2$–$RuO_2$ supported on Sb-doped $SnO_2$ nanoparticles. Electrochim Acta 2010;55:1978–84.
[22] Lee WH, Kim H. Oxidized iridium nanodendrites as catalysts for oxygen evolution reactions. Catal Commun 2011;12:408–11.
[23] Schmidt TJ, Gasteiger HA, Stab GD, Urban PM, Kolb DM, Behm RJ. Characterization of high-surface-area electrocatalysts using a rotating disk electrode configuration. J Electrochem Soc 1998;145:2354–8.
[24] Hackett K, Verhoef S, Cutler RA, Shetty DK. Phase constitution and mechanical properties of carbides in the Ta–C system. J Am Ceram Soc 2009;92:2404–7.
[25] He Y, Zhu Y, Wu N. Synthesis of nanosized $NaTaO_3$ in low temperature and its photocatalytic performance. J Solid State Chem 2004;177:3868–72.
[26] Scherrer P. Bestimmung der grösse und der inneren struktur von kolloidteilchen mittels röntgenstrahlen. Nachrichten Göttinger Gesellschaft 1918;2:98–100.
[27] Roginskaya YE, Varlamova TV, Goldstein MD, Belova ID, Galyamov BS, Shifrina RR, et al. Formation, structure and electrochemical properties of $IrO_2$–$RuO_2$ oxide electrodes. Mater Chem Phys 1991;30:101–13.
[28] De Pauli CP, Trasatti S. Electrochemical surface characterization of $IrO_2 + SnO_2$ mixed oxide electrocatalysts. J Electroanal Chem 1995;396:161–8.
[29] Bockris JO'M. Kinetics of activation controlled consecutive electrochemical reactions: anodic evolution of oxygen. J Chem Phys 1956;24:817–27.
[30] Matsumoto Y, Sato E. Electrocatalytic properties of transition metal oxides for oxygen evolution. Mater Chem Phys 1986;14:397–426.
[31] Da Silva LM, Boodts JFC, De Faria LA. Oxygen evolution at $RuO_2(x) + Co_3O_4(1 - x)$ electrodes from acid solution. Electrochim Acta 2001;46:1369–75.